Published in J. Opt. Soc. Am. A, Vol. 18 No. 4 pp. 862–872, April 2001.

Myopic deconvolution from wave-front sensing

L. M. Mugnier, C. Robert, J.-M. Conan, V. Michau and S. Salem *

Office National d'Études et de Recherches Aérospatiales (ONERA)
Optics Department, BP 72, F-92322 Châtillon cedex, France

Deconvolution from wave-front sensing is a powerful and low-cost high-resolution imaging technique designed to compensate for the image degradation due to atmospheric turbulence. It is based on a simultaneous recording of short-exposure images and wave-front sensor (WFS) data. Conventional data processing consists of a sequential estimation of the wave fronts given the WFS data and then of the object given the reconstructed wave fronts and the images. However, the object estimation does not take into account the wave-front reconstruction errors. A joint estimation of the object and the respective wave fronts has therefore been proposed to overcome this limitation. The aim of our study is to derive and validate a robust joint estimation approach, called myopic deconvolution from wave-front sensing. Our estimator uses all data simultaneously in a coherent Bayesian framework. It takes into account the noise in the images and in the WFS measurements and the available *a priori* information on the object to be restored as well as on the wave fronts. Regarding the *a priori* information on the object, an edge-preserving prior is implemented and validated. This method is validated on simulations and on experimental astronomical data.

OCIS codes: atmospheric turbulence 010.1330, wave-front sensing 010.7350, deconvolution 100.1830, image reconstruction-restoration 100.3020, inverse problems 100.3190, telescopes 110.6770.

1. INTRODUCTION

The performance of high-resolution imaging with large optical instruments is severely limited by atmospheric turbulence. Deconvolution from wave-front sensing (DWFS) is a powerful high-resolution imaging technique designed to compensate for the image degradation due to atmospheric turbulence. It can be an interesting, light-weight, and low-cost alternative to adaptive optics. It is based on a simultaneous recording of monochromatic short-exposure images and associated wave-front sensor (WFS) data. This technique was originally proposed by Fontanella in 1985 [1]. The conventional data processing consists of a sequential estimation of the wave fronts given the WFS data and then of the object given the reconstructed wave fronts and the images. This estimator was tested by Primot *et al.* on laboratory data[2, 3]. The first astronomical results were obtained in the early 1990's[4, 5]. Primot[3] also gave an analytical expression of the signal-to-noise ratio (SNR) of the technique. DFWS should be more efficient than speckle interferometry for two reasons: DWFS is not limited by speckle noise at high flux[6] and the SNR is better for extended objects, provided that a bright source is available for the WFS. This second point was confirmed in recent publications[7, 8]. The estimator proposed by Primot was, however, shown to be biased[9] since it does not take into account the wave-front reconstruction errors in object estimation. An unbiased estimator can be obtained with additional calibration data recorded on an unresolved star[10] but its high-flux performance is limited by speckle noise[11]. An alternative approach is to perform a joint estimation of the object and the wave fronts, accounting for the noise both in the images and in the WFS data[11, 12, 13, 14].

The aim of this paper is to propose a robust joint estimator derived in a Bayesian framework that takes advantage of all the available statistical information: the noise statistics in the images and in the WFS as well as the available *a priori* knowledge about the object structure and about the turbulent-phase statistics. This novel method, recently presented in Ref. [15], is called myopic deconvolution from wave-front sensing (MDWFS).

The idea of using WFS data and images jointly can be found in the pioneering work of Schulz[12]. Our contribution is twofold: first, we model our WFS data as slopes deduced from wide-band images, not as narrow-band images. This is mandatory for the processing of low-flux experimental data ; indeed, in DWFS all the photons not used for speckle imaging (which is necessarily narrow band) can and should be used for wave-front sensing. Second, we incorporate regularization into the data processing, for both the phase and the object. More specifically, our approach is a joint (object and phase) maximum *a posteriori* (MAP) estimation, which is more robust to noise than an unregularized maximum-likelihood estimation. The prior on the turbulent phase is derived from Kolmogorov statistics. The prior used to regularize the estimation of the object can be taken as Gaussian, in which case the Bayesian interpretation of regularization provides a means to avoid any manual tuning of a regularization

*Other author information: Email: authorname@onera.fr ; URL: http://www.onera.fr/dota

parameter. As an alternative, an edge-preserving object prior is also implemented and validated; it is particularly suitable for restoring asteroids or man-made objects such as satellites.

We use the term myopic deconvolution instead of blind deconvolution to underline the fact that during the deconvolution, the phase is neither completely unknown (WFS measurements are used) nor assumed to be perfectly known through the WFS measurements.

The outline is as follows. The imaging models for the images and for the WFS are presented in Section 2. In Section 3 we recall the conventional framework of DWFS, which consists of a sequential estimation of (a) the wave fronts, given the WFS data, and (b) the object, given the wave-front estimates and the images; we also introduce the various terms of the criteria that can be minimized in this sequential estimation for optimal wave-front estimation and for edge-preserving object restoration. Then in Section 4 we introduce our myopic deconvolution approach, which replaces the two previous minimizations (wave-front estimation and object estimation) with a single joint minimization. This scheme is validated by simulations in Section 5 for the case of satellite imaging, and some experimental results are given in Section 6.

2. IMAGING MODEL AND PROBLEM STATEMENT

A linear shift-invariant model is assumed for all M recorded short-exposure images i_t of the observed object o:

$$i_t = o \star h_t + n_t, \quad 1 \leq t \leq M, \tag{1}$$

where $\star$ denotes the convolution operator, h_t is the instantaneous point spread function (PSF), at time t, of the system consisting of the atmosphere, of the telescope, and of the detector, and n_t is an additive noise (often predominantly photon noise). The shift-invariance assumption is valid if the field of view is within the isoplanatic patch. If the field of view is larger, then the phase variations in the field should be modeled, taking into account possible wave-front measurements in different directions as well as *a priori* information on the wave-front spatial variations 16, 17.

The integration time of each image is considered to be short enough (typically 10 ms or less) to "freeze" the turbulence. Assuming that scintillation is negligible (near-field approximation), the PSF at time t is completely characterized by the turbulent phase φ_t in the pupil of the instrument:

$$h_t = |\mathrm{FT}^{-1}[P \exp(j\varphi_t)]|^2, \tag{2}$$

where P is the pupil function (1 inside, 0 outside) and FT denotes Fourier transformation. Owing to this relationship, which will be used throughout the paper, the knowledge of the wave front φ_t is equivalent to that of the PSF h_t. The phase is decomposed on the basis of Zernike polynomials 18 $\{Z_k\}$:

$$\varphi_t(r) = \sum_k \phi_t^k Z_k(r), \tag{3}$$

so the unknown phase at time t is the vector $\boldsymbol{\phi}_t = (\phi_t^1, \ldots, \phi_t^k, \ldots)^T$, where T denotes transposition. In practice the summation on k will be limited to some high number K (typically one hundred to a few hundreds) chosen to keep the computational burden reasonable. The turbulent phase in the pupil is considered zero-mean Gaussian with Kolmogorov statistics; its covariance matrix C_ϕ is thus known and given by Noll's formula 18.

In the following sections we shall consider that the object and the image are sampled on a regular grid, hence a vectorial formulation for Eq. (1):

$$\mathbf{i}_t = \mathbf{o} \star \mathbf{h}_t + \mathbf{n}_t = \mathcal{H}_t \mathbf{o} + \mathbf{n}_t, \tag{4}$$

where $\mathbf{o}$, $\mathbf{i}_t$ and $\mathbf{n}_t$ are the vectors corresponding to the lexicographically ordered object, image, and zero-mean noise, respectively. $\mathcal{H}_t$ is the Toeplitz matrix corresponding to the convolution by the PSF $\mathbf{h}_t$.

The WFS is assumed to be working in a linear domain, which is very reasonable for the Shack-Hartmann (SH) WFS considered in this paper. The WFS data recorded at time t can thus be written as:

$$\mathbf{s}_t = \mathcal{D}\boldsymbol{\phi}_t + \mathbf{n'}_t, \tag{5}$$

where $\mathbf{s}_t$ is the vector concatenating the WFS measurements (wave-front slopes in the case of a SH sensor), $\mathbf{n'}_t$ is a zero-mean Gaussian noise (of covariance $C_{n'}$), $\boldsymbol{\phi}_t$ is the turbulent phase vector, and $\mathcal{D}$ is the so-called interaction matrix, which depends

on the chosen WFS and on its geometrical configuration as well as on the basis chosen for $\boldsymbol{\phi}$. For example, for a SH WFS and a phase decomposed on the Zernike polynomials, the columns of $\mathcal{D}$ consist of the collection of the responses of the WFS to each Zernike polynomial, which are close to the spatial derivatives of these polynomials 3.

The problem at hand is to estimate the observed object $\mathbf{o}$ given a set of images $\mathbf{i}_t$ and a synchronously recorded set of wave-front measurements $\mathbf{s}_t$ $(1 \leq t \leq M)$.

3. SEQUENTIAL ESTIMATION OF WAVE FRONTS AND OBJECT

The conventional processing of DWFS data consists of a sequential estimation of the wave fronts, given the WFS data, and then of the object, given the reconstructed wave fronts (and thus the PSF's) and the images. Both the wave-front reconstruction and the image restoration are ill-posed inverse problems and must be regularized (see Refs. 19 and 20 for reviews on regularization), in the sense that some *a priori* information must be introduced in their resolution for the solution to be unique and robust to noise.

A. Wave-Front Reconstruction

Let us first tackle the wave-front reconstruction problem. A common solution for the estimation of a wave front $\boldsymbol{\phi}$ given slope measurements $\mathbf{s}$ made by a SH WFS is the least squares one:

$$\hat{\boldsymbol{\phi}} = (\mathcal{D}^T\mathcal{D})^{-1}\mathcal{D}^T\mathbf{s}. \tag{6}$$

This solution can be interpreted as a maximum-likelihood solution if the noise on the WFS is stationary white Gaussian. The matrix $\mathcal{D}^T\mathcal{D}$ is often ill-conditioned or even not invertible, because the number of measurements is finite (twice the number of subapertures N_{sub}) whereas the dimension of the true phase vector $\boldsymbol{\phi}$ is theoretically infinite (in practice a high number K, possibly greater than $2N_{sub}$). The usual remedy is to reduce the dimension K of the vector space of the unknown $\boldsymbol{\phi}$. This kind of regularization is not very satisfactory because the choice of the dimension is difficult and somewhat *ad hoc*: the best choice depends in particular on the SNR of the WFS. A more rigorous approach is to turn to a probabilistic solution that makes use of prior information on the turbulent phase. Such a solution is, for instance, the linear minimum-variance estimator proposed by Wallner 21 (similar to the Wiener filter familiar in image restoration) and first applied to DWFS by Welsh and VonNiederhausern 22. Another such solution is given by a MAP approach, i.e., by searching for the most likely phase given the measurements and our prior information. When, as in this paper, the noise and the turbulent phase are considered Gaussian, these two approaches are equivalent 23. The maximization of the posterior probability of the phase is equivalent to the minimization of the neg-log-posterior probability of $\boldsymbol{\phi}$, called J^{ϕ}_{MAP} in the following. With use of Bayes' rule, it is straightforward to show that J^{ϕ}_{MAP} takes the following form:

$$J^{\phi}_{MAP} = J_s + J_{\phi}, \quad \text{where} \tag{7}$$

$$J_s = \frac{1}{2}(\mathbf{s} - \mathcal{D}\boldsymbol{\phi})^T C_{n'}^{-1}(\mathbf{s} - \mathcal{D}\boldsymbol{\phi}) \quad \text{and} \tag{8}$$

$$J_{\phi} = \frac{1}{2}\boldsymbol{\phi}^T C_{\phi}^{-1}\boldsymbol{\phi}. \tag{9}$$

J_s is a term of fidelity to the WFS data and is the opposite of their log-likelihood, and J_{ϕ} is a term of fidelity to the prior. The solution is analytical and can be written in matrix form 24 as follows:

$$\hat{\boldsymbol{\phi}}_{MAP} = (\mathcal{D}^T C_{n'}^{-1}\mathcal{D} + C_{\phi}^{-1})^{-1}\mathcal{D}^T C_{n'}^{-1}\mathbf{s}. \tag{10}$$

Note that there is a equivalent expression for this solution that involves the inversion of a smaller matrix when the phase $\boldsymbol{\phi}$ is expanded on more modes than there are WFS measurements:

$$\hat{\boldsymbol{\phi}}_{MAP} = C_{\phi}\mathcal{D}^T(\mathcal{D}C_{\phi}\mathcal{D}^T + C_{n'})^{-1}\mathbf{s}. \tag{11}$$

This phase estimate is more accurate than the least squares one of Eq. (6), and additionally does not require an *ad hoc* tuning of the dimension K of the unknown phase. To the best of our knowledge, the phase estimate has so far always been used as

the true phase [for computing the PSF's by use of Eq. (2)] for the image restoration 8, 9, 10. In contrast, the phase estimate of Eq. (10) will be used as a *starting point* for our myopic method, and the corresponding criterion of Eq. (7) will be *part* of the criterion derived in the myopic method. We delay the presentation of this myopic method to the following section and for the time being we consider, as is classically done, that the wave fronts estimated by the MAP approach above are the true ones.

B. Multiframe Image Restoration

Let us now turn to the image restoration problem, in the classical setting where the PSF's are known. Most deconvolution techniques boil down to the minimization (or maximization) of a criterion. The first issue is the definition of a suitable criterion for the given inverse problem. The second issue is then to find the position of the criterion's global minimum which is defined as the solution. In some rare cases (when the criterion to be minimized is quadratic) the solution is given by an analytical expression (e.g., Wiener filtering), but most of the time one must resort to an iterative numerical method to solve the problem. For our applications we use a conjugate-gradient method.

Similarly to wave-front reconstruction, a common approach for the image restoration is to use a (multiframe) least squares. The solution, i.e., the minimum of this criterion, is analytical and is the multiframe inverse filter proposed in DWFS by Primot *et al.* 3. This approach has a maximum likelihood interpretation when the noise can be assumed to be stationary white Gaussian. It leads to unacceptable noise amplification for high noise levels and must therefore be regularized.

A natural way to regularize the inversion is functional regularization. It consists in defining the solution as the minimum of a compound criterion with two terms, say $J_i + \lambda J_o$. Term J_i of the criterion enforces fidelity to the data (it can be, e.g., a least squares) while term J_o expresses fidelity to some prior information about the solution. Two choices must be made: one is the regularization functional, i.e., the expression of J_o, and the other is the regularization parameter λ, a scalar that adjusts the tradeoff between the two terms.

The choice of the regularization parameter can be made automatically during the restoration process in a constrained least squares formulation of the regularization 25. Yet, the regularization functional remains to be chosen by the user in a somewhat arbitrary fashion.

An alternative is to use the Bayesian interpretation of regularization, which can provide "natural" regularization functionals. This is the approach taken in this paper: the object is endowed with an *a priori* distribution $p(\mathbf{o})$, and Bayes' rule combines the likelihood of the M images $p(\{\mathbf{i}_t\}_{t=1}^M|\mathbf{o},\{\boldsymbol{\phi}_t\}_{t=1}^M)$ with this *a priori* distribution into the *a posteriori* probability distribution $p(\mathbf{o}|\{\mathbf{i}_t\}_{t=1}^M,\{\boldsymbol{\phi}_t\}_{t=1}^M)$:

$$p(\mathbf{o}|\{\mathbf{i}_t\}_{t=1}^M,\{\boldsymbol{\phi}_t\}_{t=1}^M) \propto p(\{\mathbf{i}_t\}_{t=1}^M|\mathbf{o},\{\boldsymbol{\phi}_t\}_{t=1}^M) \times p(\mathbf{o}), \tag{12}$$

We shall make two assumptions in the following: First, that the noise is independent between images and second, that the time between two successive data recordings is greater than the typical evolution time of turbulence. With these two reasonable assumptions, the likelihood of the set of images can be rewritten as the product of the likelihoods of the individual images, each of them conditioned only by the object and by the true phase at the same time. The restored object is defined as the most probable one given the data, i.e., the one that minimizes:

$$J_{MAP}^o(\mathbf{o}) = \sum_{t=1}^{M} J_i(\mathbf{o};\boldsymbol{\phi}_t,\mathbf{i}_t) + J_o(\mathbf{o}), \tag{13}$$

where

$$J_i(\mathbf{o};\boldsymbol{\phi}_t,\mathbf{i}_t) = -\ln p(\mathbf{i}_t|\mathbf{o},\boldsymbol{\phi}_t) \text{ and} \tag{14}$$

$$J_o(\mathbf{o}) = -\ln p(\mathbf{o}). \tag{15}$$

J_i is the neg-log-likelihood of image number t and J_o is the neg-log-prior probability of the object. The minimization of this criterion is performed on $\mathbf{o}$ only, and the $\boldsymbol{\phi}_t$'s are a reminder of the dependency of the criterion on the phases, assumed here to be known. The forms taken by criteria J_i and J_o depend on the statistical assumptions made on the noise and on the object, respectively, and are discussed next.

1. Noise Statistics

If the noise is zero mean Gaussian with covariance matrix C_n, then J_i is quadratic for any image $\mathbf{i}$:

$$J_i(\mathbf{o};\boldsymbol{\phi},\mathbf{i}) = \frac{1}{2}(\mathbf{h}\star\mathbf{o}-\mathbf{i})^T C_n^{-1}(\mathbf{h}\star\mathbf{o}-\mathbf{i}), \tag{16}$$

which depends on $\boldsymbol{\phi}$ through $\mathbf{h}$ (see Eq. (2)). In particular, if the noise is, in addition, stationary and white, of variance σ_n^2, then Eq. (16) reduces to the familiar least squares:

$$J_i(\mathbf{o};\boldsymbol{\phi},\mathbf{i}) = \frac{1}{2\sigma_n^2}\|\mathbf{h}\star\mathbf{o}-\mathbf{i})\|^2 = \sum_{l,m}\left|[\mathbf{h}\star\mathbf{o}]\,(l,m)-\mathbf{i}(l,m)\right|^2 \tag{17}$$

In astronomical imaging, the noise is often predominantly photon noise, which follows Poisson statistics. One possibility is then to derive the true MAP criterion for photon noise statistics, which is the neg-log-likelihood of the Poisson law. In this paper J_i is taken for simplicity as the least-squares term of Eq. (17) with a uniform noise variance equal to the mean number of photons per pixel. This can be considered as a first approximation of the photon noise in the case of a rather bright and extended object.

2. Object Prior

The choice of a Gaussian prior probability distribution for the object can be justified from an information theory standpoint as being the least informative, given the first two moments of the distribution. In this case a reasonable model of the object's power spectral density (PSD) can be found 26 and used to derive the criterion J_o. This is more satisfactory than an *ad hoc* regularization functional such as the identity or the traditional Laplacian and gives better object estimates 26. In addition, because J_o is derived from a probability distribution, there is no regularization parameter (scaling factor between the J_i's and J_o) to be adjusted. Finally, the solution is analytical and is a multiframe Wiener filter 27.

The disadvantage of a Gaussian prior, especially for objects with sharp edges such as asteroids or artificial satellites, is that it tends to oversmooth edges. A possible remedy is to use an edge-preserving prior such as an L_2–L_1 criterion, quadratic for small gradients and linear for large ones 28. The quadratic part ensures a good smoothing of the small gradients (i.e., of noise), and the linear behavior cancels the penalization of large gradients (i.e., of edges) 29. Here we use a function that is an isotropic version of the expression suggested by Rey 30 in the context of robust estimation, used by Brette and Idier 31 for image restoration, and recently applied to imaging through turbulence 32:

$$J_o(\mathbf{o}) = \mu\,\delta^2\sum_{l,m}\left[\left(\frac{\nabla\mathbf{o}(l,m)}{\delta}\right)-\ln\left(1+\frac{\nabla\mathbf{o}(l,m)}{\delta}\right)\right], \tag{18}$$

where $\nabla\mathbf{o}(l,m) = [\nabla_x\mathbf{o}(l,m)^2+\nabla_y\mathbf{o}(l,m)^2]^{1/2}$, and $\nabla_x\mathbf{o}$ and $\nabla_y\mathbf{o}$ are the object finite-difference gradients along x and y, respectively.

The global factor μ and the threshold δ have to be adjusted according to the noise level and the structure of the object. This is currently done by hand but an automatic procedure is under study. This function is convex, as is the global criterion, which ensures uniqueness and stability of the solution with respect to noise and also justifies the use of a gradient-based method for the minimization. Note that if the object is a stellar field, then a stronger prior can be used, namely, the fact that the unknown object is a collection of Dirac delta functions 33.

4. JOINT ESTIMATION OF WAVE FRONTS AND OBJECT

A. Motivation

The conventional processing of DWFS data consists of a sequential estimation of the wave fronts given the WFS data and then of the object given the images and the reconstructed wave fronts, which are regarded as the true ones. So, obviously, the information about the wave fronts is gathered only in the WFS data, not in the images.

Yet the wave-front estimates are inevitably noisy, so it would be useful to exploit both the WFS data and the images in the wave-front estimation. And there *is* some exploitable information about the wave front (or the PSF) in a short-exposure turbulence-degraded image. To prove this point, it is enough to recall that multiframe blind deconvolution for such images (blind meaning without a WFS) is feasible, at least at high SNR's; indeed the PSF reparameterization of Eq. (2) by the phase, which was proposed by Schulz 34, is a strong constraint that allows this technique to work in practice, even on experimental data 34, 35.

A drawback of blind criteria is that they usually exhibit local minima, and the PSF reparameterization by the phase is probably not a strong enough constraint to give the blind-deconvolution problem a unique solution. So the WFS data should definitely not be thrown away but rather used in conjunction with the images.

Our aim is thus to estimate the object and the PSF's while taking into account all the measurements (WFS data and images) simultaneously in a coherent framework.

B. Myopic-Deconvolution Approach

The myopic-deconvolution approach consists in a joint estimation of the object $\mathbf{o}$ and the turbulent phases $\boldsymbol{\phi}_t$ that are the most likely given the images $\mathbf{i}_t$, the WFS data $\mathbf{s}_t$ and the *a priori* information on $\mathbf{o}$ and the $\boldsymbol{\phi}_t$'s. If we use Bayes' rule in a way similar to its use in Subsection 3 B and the independence assumptions therein, the joint posterior probability distribution of the object and the phases is

$$\begin{aligned} p(\mathbf{o}, \{\boldsymbol{\phi}_t\}_{t=1}^M | \{\mathbf{i}_t\}_{t=1}^M, \{\mathbf{s}_t\}_{t=1}^M) &\propto p(\{\mathbf{i}_t\}_{t=1}^M, \{\mathbf{s}_t\}_{t=1}^M | \mathbf{o}, \{\boldsymbol{\phi}_t\}_{t=1}^M) \times p(\mathbf{o}) \times p(\{\boldsymbol{\phi}_t\}_{t=1}^M) \\ &\propto \prod_{t=1}^M p(\mathbf{i}_t | \mathbf{o}, \boldsymbol{\phi}_t) \times p(\mathbf{o}) \times \prod_{t=1}^M p(\mathbf{s}_t | \boldsymbol{\phi}_t) \times \prod_{t=1}^M p(\boldsymbol{\phi}_t). \end{aligned} \tag{19}$$

So the joint MAP estimates $(\hat{\mathbf{o}}, \{\hat{\boldsymbol{\phi}}_t\})$ are the ones that minimize:

$$J_{MAP}(\mathbf{o}, \{\boldsymbol{\phi}_t\}) = \sum_{t=1}^M J_i(\mathbf{o}, \boldsymbol{\phi}_t; \mathbf{i}_t) + J_o(\mathbf{o}) + \sum_{t=1}^M J_s(\boldsymbol{\phi}_t; \mathbf{s}_t) + \sum_{t=1}^M J_\phi(\boldsymbol{\phi}_t), \tag{20}$$

where

- The J_i's are terms of fidelity to image data; $J_i(\mathbf{o}, \boldsymbol{\phi}_t; \mathbf{i}_t)$ is the neg-log-likelihood of the t-th image; for a Gaussian noise, $J_i(\mathbf{o}, \boldsymbol{\phi}_t; \mathbf{i}_t) = (1/2)(\mathbf{h}_t \star \mathbf{o} - \mathbf{i}_t)^T C_n^{-1} (\mathbf{h}_t \star \mathbf{o} - \mathbf{i}_t)$, which is the same as Eq. (16) except that it is now a function of the object *and* the phases;
- $J_o(\mathbf{o})$ is the object prior, which can be taken either as quadratic (with a simple parametric model for the object PSD 26) or as an edge-preserving criterion [see Eq. (18)];
- The J_s's are terms of fidelity to WFS data; under our assumptions they are quadratic and given by Eq. (8);
- The J_ϕ's are the phase priors; for Kolmogorov statistics they, too, are quadratic and given by Eq. (9).

C. Implementation of the Myopic Deconvolution

The criterion of Eq. (20) is minimized numerically to obtain the joint MAP estimate for the object $\mathbf{o}$ and the phases $\boldsymbol{\phi}_t$. The minimization is performed on the unknown object $\mathbf{o}$ and on the unknown phases $\boldsymbol{\phi}_t$ by a fast conjugate-gradient method36. Because the criterion is continuously differentiable, the convergence of the conjugate-gradient method to a stationary point (in practice, to a local minimum) is guaranteed37. We have found that the convergence is faster if the descent direction is re-initialized regularly (typically every ten iterations for the sizes of our images and phase vectors); this result can be attributed to the fact that the criterion to be minimized is not quadratic. This modified version of the conjugate gradient is known as the *partial conjugate-gradient method* and has similar convergence properties (see Sec. 8.5 of Ref. 38).

A practical but severe minimization problem may occur if one simply stacks together the object and the phases into a vector of unknowns, because the gradients of the criterion with respect to the object and to the phase may have very different orders of magnitude. One solution can be to scale the unknown object; the scaling must be adjusted so that the gradients with respect

to the object and to the phase be of comparable magnitude[39]. We have found that it is safer and faster to split the minimization into two blocks and to alternate between minimizations on the object for the current phase estimates and minimizations on the phases for the current object estimate, so that this scaling problem is avoided. Additionally, as mentioned above we use a partial conjugate-gradient method; i.e., we perform a fixed number of conjugate-gradient iterations within each block (object or phases) and then switch to the other block.

Finally, a careful inspection of the criterion J_{MAP} of Eq. (20) allows a significant reduction of the computational burden: first, only the $M+1$ first terms of J_{MAP} depend on the object, so that the last $2M$ terms of the criterion need not be computed when minimizing on the object. Second, when J_{MAP} is minimized on the phases $\{\boldsymbol{\phi}_t\}_{t=1}^{M}$ for the current object estimate, the minimization can be decoupled into M minimizations, each being performed on one single phase screen $\boldsymbol{\phi}_t$ and involving only three terms ($J_i + J_s + J_\phi$).

As all numerical minimizations do, this one needs an initialization point or initial guess; in order both to speed up the descent and to avoid, in practice, the local minima associated with joint criteria, we use as an initial guess the MAP estimates obtained by the sequential processing described in Section 3. More precisely, the initialization phases are those obtained by a MAP processing of the sole WFS data, i.e., by the minimization of the two right-hand terms of Eq. (20); these phases are given analytically by Eq. (10). The initialization object is the one obtained by a MAP processing of the sole images given the initialization phases, i.e., by the minimization of the two left-hand terms of Eq. (20); this object has an analytical expression when both the object and the noise are assumed to be Gaussian (it is the multiframe Wiener filter applied to the image sequence).

The minimization is not stopped by hand but rather when the estimated object and phases no longer evolve (i.e., when their evolution from one iteration to the next is close to machine precision). The metric used to assess the quality of the object estimate is the standard mean square error (MSE) between the true object and the estimated one, expressed in photons per pixel. We have verified that the estimated objects are not shifted by more than a fraction of pixel with respect to the true object, so the MSE's mentioned below are a good measure of the restored object's quality.

The conjugate-gradient routine needs to repeatedly compute the criterion and its gradients with respect to the object $\mathbf{o}$ and the phases $\boldsymbol{\phi}_t$. These gradients can be computed analytically; they are given in Appendix A for completeness. The whole algorithm is summarized in the block diagram of Table 1. In the next section we validate the proposed myopic approach on simulated data.

Table 1. **Block-diagram of the Algorithm Used for Myopic Deconvolution from Wave-Front Sensing.**

Step	Operation performed	Implementation
1. Initialization	$\boldsymbol{\phi}_t^0 = \hat{\boldsymbol{\phi}}_t^{MAP} = (\mathcal{D}^T C_{n'}^{-1} \mathcal{D} + C_\phi^{-1})^{-1} \mathcal{D}^T C_{n'}^{-1} \mathbf{s}_t \quad \forall t$	matrix multiplication
	$\mathbf{o}^0 = \arg\min_{\mathbf{o}} \left(\frac{1}{2\sigma_n^2} \sum_t \|\mathbf{h}(\boldsymbol{\phi}_t^0) \star \mathbf{o} - \mathbf{i}_t\|^2 + J_o(\mathbf{o}) \right)$	1 conjugate-gradient minimization
2. q-th phase iteration	$\boldsymbol{\phi}_t^q = \arg\min_{\boldsymbol{\phi}} \big(\frac{1}{2\sigma_n^2} \|\mathbf{h}(\boldsymbol{\phi}) \star \mathbf{o}^{q-1} - \mathbf{i}_t\|^2$ $+ \frac{1}{2}(\mathbf{s}_t - \mathcal{D}\boldsymbol{\phi})^T C_{n'}^{-1} (\mathbf{s}_t - \mathcal{D}\boldsymbol{\phi}_t) + \frac{1}{2} \boldsymbol{\phi}^T C_\phi^{-1} \boldsymbol{\phi} \big)$ $\forall t, 1 \le t \le M$	M partial conjugate-gradient minimizations
3. q-th object iteration	$\mathbf{o}^q = \arg\min_{\mathbf{o}} \left(\frac{1}{2\sigma_n^2} \sum_t \|\mathbf{h}(\boldsymbol{\phi}_t^q) \star \mathbf{o} - \mathbf{i}_t\|^2 + J_o(\mathbf{o}) \right)$	1 partial conjugate-gradient minimization
4. Stopping rule	if $\|\mathbf{o}^q - \mathbf{o}^{q-1}\| > 10^{-7} \|\mathbf{o}^q\|$ or if $\exists t; \|\boldsymbol{\phi}_t^q - \boldsymbol{\phi}_t^{q-1}\| > 10^{-7} \|\boldsymbol{\phi}_t^q\|$ then go to (2), else stop.	

5. VALIDATION BY SIMULATIONS

A set of 100 noisy images and associated wave-front measurements are simulated. The 100 turbulent wave fronts are obtained with a modal method 40: The phase is expanded on the Zernike polynomial basis, and generated with Kolmogorov statistics 18; the strength of the turbulence corresponds to a ratio D/r_0 of the telescope diameter to the Fried parameter equal to 10.

Each of these turbulent wave fronts leads to a 128×128 Shannon-sampled short-exposure image with use of Eqs. (1) and (2). The image noise is a uniform Gaussian noise with a variance equal to the mean flux, or $10^4/(128 \times 128) = 0.61$ photons/pixel. It approximates the photon noise for a uniform distribution of a 10^4 photon total flux over the image sensor. Figure 1 shows the original object (a model of the SPOT satellite), one of the 100 turbulence PSF's and the corresponding noisy image.

The WFS is of SH type with 20×20 subapertures, of which 308 are useful, and without a central obscuration. A white Gaussian noise is added to the computed slopes [see Eq. (5)] so that the SNR on the measured slopes, defined as the ratio of the turbulence slope variance over the noise variance, is 1.

The Zernike expansion of the phase is limited to 190 Zernike polynomials (radial degree 18) only to keep the computational burden reasonably small; indeed, with the SNR chosen for the WFS, it can be shown that the reconstructed phase modes and the reconstructed noise have the same level for the 55th polynomial (radial degree 9).

Figure 2 compares the conventional sequential estimation and our myopic estimation for the same Gaussian object model with the same PSD. On the left, the conventional restoration, consisting of a MAP wave-front estimation followed by a multiframe Wiener filter, gives a MSE of 0.48 photon. On the right, the myopic joint estimation gives a MSE on the object of 0.45 photon. Several details are visibly better restored on the myopic restoration, in particular the two little bright rectangles near the dish and the separations between the solar panels. Figure 3 shows the same comparison between the conventional and the myopic restorations (left and right, respectively), but with the edge-preserving prior of Eq. (18) plus a positivity constraint instead of the Gaussian prior. The MSE is 0.45 photon and 0.39 photon, respectively. A particularly noticeable difference between these two images is the thin shadow on the lower left part of the satellite body, which is visible only in the edge-preserving myopic restoration. In both cases the images restored with our myopic method (right side of Figs. 2 and 3) are less blurred than the ones restored with the sequential scheme (left side of the same figures). And the two restorations obtained with the edge-preserving prior are also crisper and closer to the true object than are their quadratic counterparts. The restorations shown in Fig. 3 were obtained with respectively 210 s and 1450 s of CPU time on a Sun Sparc. Processing 100 frames with MDWFS therefore leads to a quite reasonable computation time.

It is remarkable that, simultaneously with the better object estimation, the myopic deconvolution provides a better estimation of the phase. We believe that the latter is due to the fact that all the available data, images included, are used for the phase estimation. A more quantitative explanation of this improvement remains to be done and is worth further study. This estimation improvement is shown in Fig. 4; the tip-tilt, the defocus, and the astigmatism happen to be particularly better estimated than by use solely of WFS data. One can note that the use of a prior that is well suited to the object (an L_2–L_1 criterion for an object that is known to have sharp edges) enhances not only the object restoration but also the phase estimation.

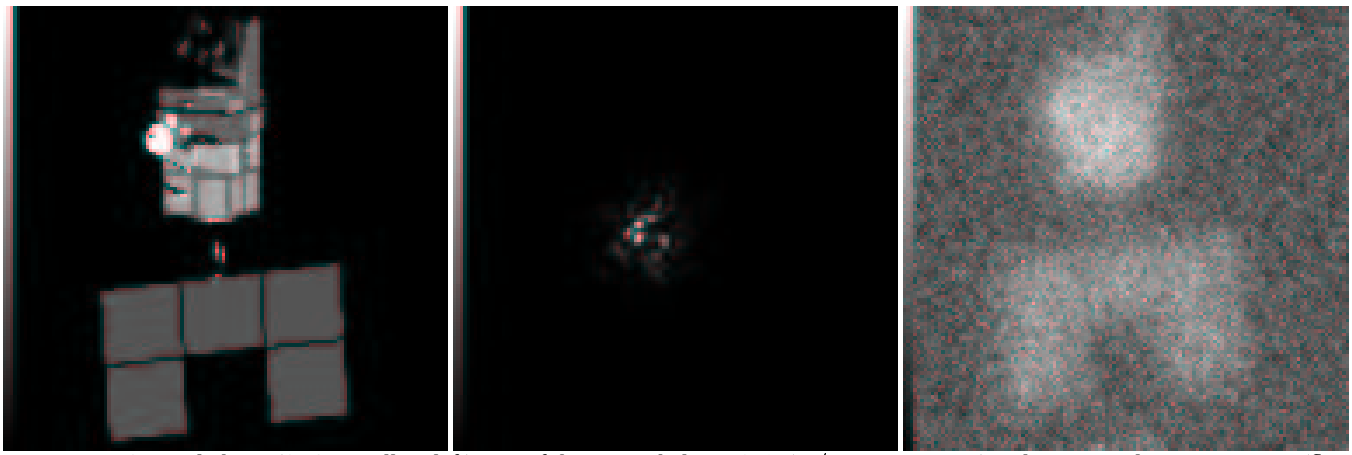

Fig. 1. Original object (SPOT satellite, left), one of the 100 turbulent PSF's ($D/r_0 = 10$, center) and corresponding noisy image (flux of 10^4 photons, right).

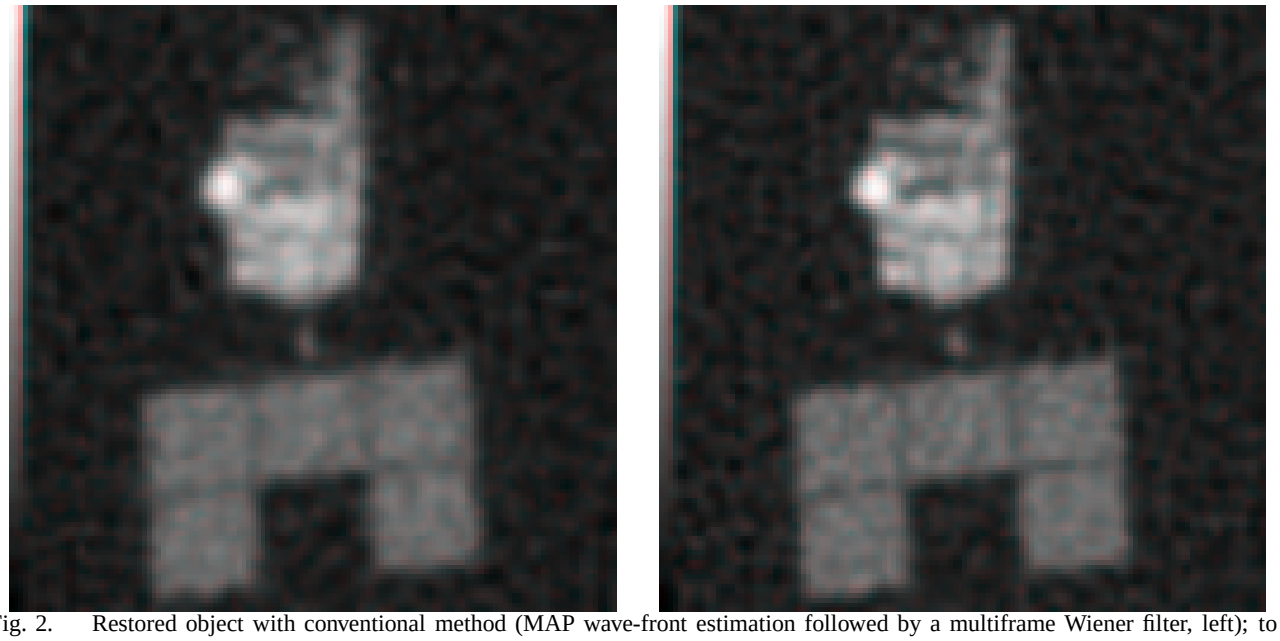

Fig. 2. Restored object with conventional method (MAP wave-front estimation followed by a multiframe Wiener filter, left); to be compared with the restored object by myopic deconvolution (right). In both cases the same Gaussian prior is used for the object. The MSE is 0.48 photons and 0.45 photons respectively.

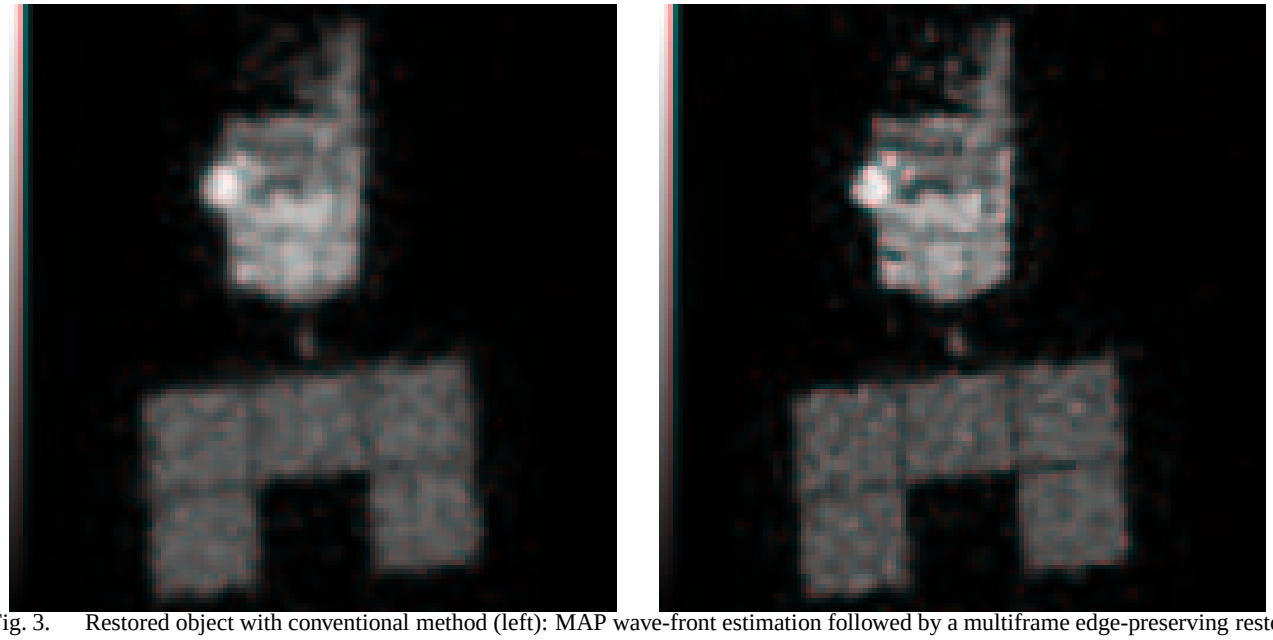

Fig. 3. Restored object with conventional method (left): MAP wave-front estimation followed by a multiframe edge-preserving restoration. Restored object by myopic deconvolution (right). In both cases the same edge-preserving prior is used for the object, with an additional positivity constraint. The MSE is 0.45 photons and 0.39 photons respectively.

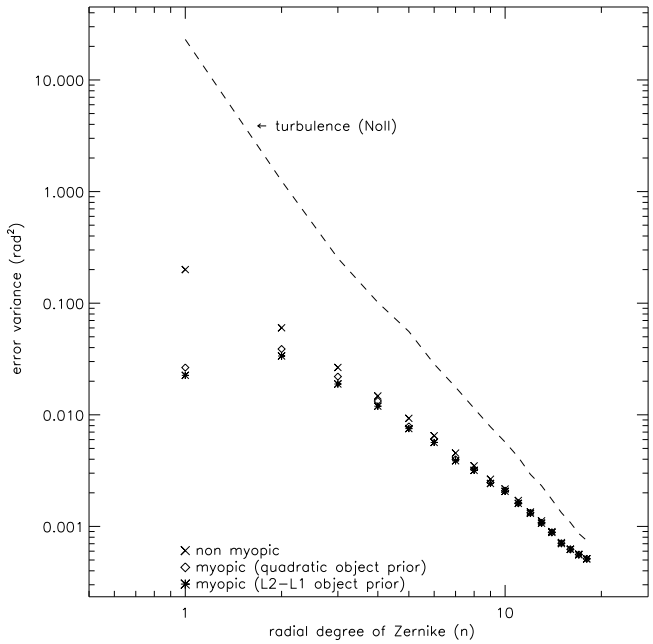

Fig. 4. Comparison of the reconstructed phase errors, as a function of the Zernike mode radial degree, for the conventional (MAP) and myopic (joint MAP) restoration schemes. The turbulent phase variance is shown for comparison (dashed line).

6. EXPERIMENTAL RESULTS

We have applied our MDWFS method to experimental images of the binary star Capella taken at the 4.2-m William Herschel Telescope, located at La Palma in the Canary Islands. Ten short-exposure images of size 128×128 were taken on November 8, 1990 at 4:00 universal time and processed. The exposure time is 5 ms on both the imaging and the wave-front sensing channel. Note that for fainter objects it has been shown that in speckle imaging it can be useful to increase the exposure time so as to obtain a better SNR in the images41, even though the speckles get blurred. Preliminary internal studies tend to show that this is not the case for DWFS, because the wave-front measurements degrade quickly when the exposure time is greater than the evolution time of turbulence.

The experimental conditions were the following: A flux of $67,500$ photons per frame and an estimated D/r_0 of 13. The imaging wavelength was $0.66\,\mu$m, which gives a diffraction-limit resolution λ/D of 32.10^{-3} arc sec. The WFS is of Shack-Hartmann type with 29×29 subapertures, of which 560 are useful because of the telescope's $29\,\%$ central obscuration. The estimated WFS SNR is 5, which gives the WFS noise level required in J_s. Note that the noise level can be artificially increased to account for non common-path aberrations in the optical setup. When this noise level goes to infinity the algorithm becomes a multi-frame regularized blind deconvolution. Figure 5 shows one of the ten processed short exposures (left), and the corresponding computed long exposure obtained by adding the ten short exposures (right); the latter image illustrates the loss in resolution associated with the long exposure.

The left panel of Fig. 6 shows the result of conventional estimation: A multiframe Wiener filter was applied to the images, with wave-front estimates obtained by a MAP reconstruction from the slopes. The PSD is taken as a constant, as is natural for a spike-like object, and the wave front is reconstructed on the first 190 Zernike polynomials. The binary nature of the star is not clearly visible. The center panel of Fig. 6 shows an improved conventional estimation, in which we have used the same flat PSD but added a positivity constraint to the restoration. The binary nature of the star begins to be visible but the binary star is still embedded in strong fluctuations.

The right panel of Fig. 6 shows the result of our MDWFS method: The object and the wave fronts are jointly estimated by minimizing the criterion of Eq. (20); the prior used is the same flat PSD with the positivity constraint, and the starting point of the minimization is the estimate on the center. There is a clear gain in image quality with the MDWFS method. In particular, the two components of Capella are clearly resolved, and the estimated angular separation is 57.10^{-3} arc sec, in good agreement with the one predicted by orbit data at the date of the experiment (55.10^{-3} arc sec).

The PSD used in the regularization is the same for the conventional and for the myopic estimations: It is deduced from the average flux in the images and is not tuned manually; one may consider underestimating the PSD (i.e., performing overregularization) to make the conventional estimation smoother, but no manual tuning of the PSD can make the conventionally restored images both sharp and free from spurious ripples.

The restoration of Capella without the use of WFS data by use of the bispectrum has also been reported 42, but such higher-order methods usually require many more images to produce a result of similar quality (typically 100 images even for very simple objects such as a binary star).

The conventional restoration with positivity constraint (center panel of Fig. 6) required 40 s of CPU time, and the myopic restoration (right part of the figure) took 110 s, which remains fairly fast.

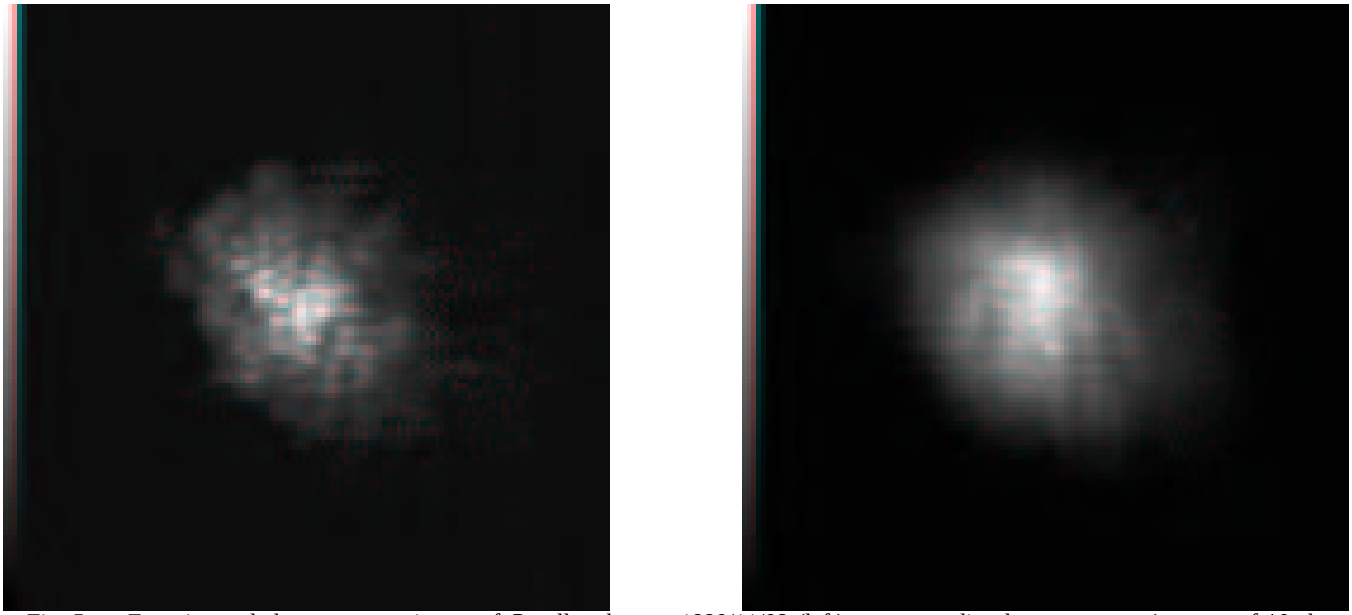

Fig. 5. Experimental short-exposure image of Capella taken on 1990/11/08 (left); corresponding long exposure (average of 10 short exposures, right).

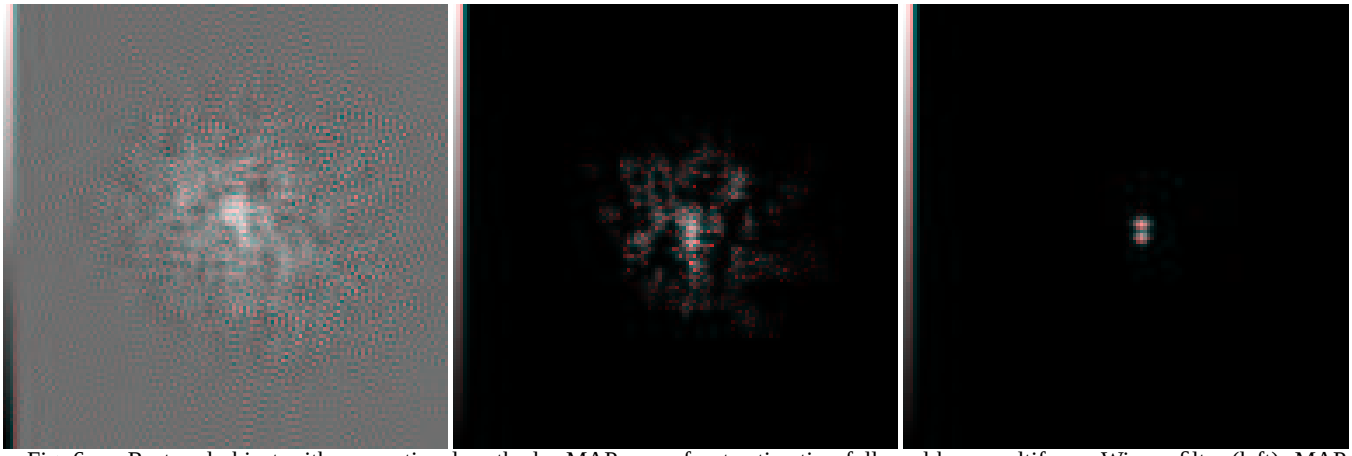

Fig. 6. Restored object with conventional methods: MAP wave-front estimation followed by a multiframe Wiener filter (left); MAP wave-front estimation followed by a quadratic restoration with a positivity constraint (center); to be compared with the object restored by the myopic deconvolution (right), using the same quadratic regularization and the same positivity constraint.

7. CONCLUSION

We have presented a novel approach for deconvolution from wave-front sensing, called myopic deconvolution from wave-front sensing (MDWFS). This approach consists in a joint estimation of the object of interest and the unknown turbulent phases; it considers all the data (WFS slopes and images) simultaneously in a coherent Bayesian framework. This method takes into account the noise in the images and in the wave-front sensor measurements, as well as the available prior information on the object to be restored and on the turbulent phases.

This approach has been validated on simulations and has led to a better object estimation than that obtained with the sequential processing of the WFS data and the images. An edge-preserving object prior has been implemented and should be very effective for asteroids or man-made objects such as satellites. An initial experimental astronomical application of MDWFS on Capella has also been presented.

Appendix A: DERIVATION OF THE GRADIENTS WITH RESPECT TO OBJECT AND PHASE PARAMETERS

The image deconvolutions shown in this paper, whether conventional or myopic, are performed by means of a conjugate-gradient routine. This routine needs to repeatedly compute the considered criterion and its gradients with respect to the object $\mathbf{o}$ (and with respect to the phases $\boldsymbol{\phi}_t$ in the case of myopic deconvolution). The gradients of all the terms of the criteria considered here are given below.

1. Gradients of the Image Data Term

The gradient of the least squares criterion $J_i(\mathbf{o}, \boldsymbol{\phi}_t; \mathbf{i}_t)$ with respect to the unknown object is easily computed in matrix form, and can be expressed in Fourier space for implementation by FFT:

$$\frac{dJ_i}{d\mathbf{o}} = \frac{1}{\sigma_n^2}\mathcal{H}_t^T(\mathcal{H}_t\mathbf{o} - \mathbf{i}_t) = \frac{1}{\sigma_n^2}FT^{-1}\left(\tilde{\mathbf{h}}_t^*\,(\tilde{\mathbf{h}}_t\,\tilde{\mathbf{o}} - \tilde{\mathbf{i}}_t)\right), \tag{A1}$$

where $\tilde{.}$ and $FT^{-1}(.)$ denote Fourier transformation and its inverse respectively.

The gradient of the least squares criterion $J_i(\mathbf{o}, \boldsymbol{\phi}_t; \mathbf{i}_t)$ with respect to the unknown phase $\boldsymbol{\phi}_t$ is done in three steps. The derivation begins by calculating the gradient of J_i with respect to the PSF $\mathbf{h}_t$:

$$\frac{dJ_i}{d\mathbf{h}_t} = \frac{1}{\sigma_n^2}FT^{-1}\left(\tilde{\mathbf{o}}^*\,(\tilde{\mathbf{h}}_t\,\tilde{\mathbf{o}} - \tilde{\mathbf{i}}_t)\right) \tag{A2}$$

It then consists in calculating the gradient of the PSF with respect to the phase $\varphi_t(l,m)$ at pixel (l,m) the pupil, and applying the chain rule. The result, already derived in 35 in a slightly different form, is:

$$\frac{dJ_i}{d\varphi_t(l,m)} = \frac{2}{A}\,\Im\{P(l,m)e^{-j\varphi_t(l,m)}\,\left[FT\left(\frac{dJ_i}{d\mathbf{h}_t}\right)\star Pe^{j\varphi_t}\right](l,m)\} \tag{A3}$$

where A is the area of the pupil (numerically, the number of pixels where $P(l,m) = 1$), $\Im$ denotes the imaginary part of a complex number and $\star$ denotes a convolution operator.

Finally, because we expand the unknown phases on the Zernike basis, we need the gradient of J_i with respect to the Zernike coefficients ϕ_t^k of phase ϕ_t; it is easily deduced from the previous expression:

$$\frac{dJ_i}{d\phi_t^k} = \sum_{l,m}\frac{dJ_i}{d\varphi_t(l,m)}\,Z_k(l,m) = \frac{2}{A}\sum_{l,m}Z_k(l,m)\,\Im\{P(l,m)e^{-j\varphi_t(l,m)}\,\left[FT\left(\frac{dJ_i}{d\mathbf{h}_t}\right)\star Pe^{j\varphi_t}\right](l,m)\} \tag{A4}$$

For a Poisson model of the image noise, the gradient of the corresponding criterion J_i could be derived similarly 43.

2. Gradient of the Object Prior Term

The gradient of the edge-preserving prior of Eq. (18) can be derived and implemented using the finite difference operators $(\nabla_x \mathbf{o})(l,m) = o(l,m) - o(l-1,m)$ and $(\nabla_y \mathbf{o})(l,m) = o(l,m) - o(l,m-1)$. One can show that:

$$\frac{dJ_o}{d\mathbf{o}} = \mu \left[\nabla_x^T \left(\frac{\nabla_x \mathbf{o}}{1 + \sqrt{(\nabla_x \mathbf{o})^2 + (\nabla_y \mathbf{o})^2}/\delta} \right) + \nabla_y^T \left(\frac{\nabla_y \mathbf{o}}{1 + \sqrt{(\nabla_x \mathbf{o})^2 + (\nabla_y \mathbf{o})^2}/\delta} \right) \right], \tag{A5}$$

where $\dot{-}$ denotes pointwise division, $(\nabla_x^T \mathbf{o})(l,m) = o(l,m) - o(l+1,m)$ and $(\nabla_y^T \mathbf{o})(l,m) = o(l,m) - o(l,m+1)$.

3. Gradients of the Slope Data and of the Phase Prior Terms

The gradient of criterion J_s is straightforward to compute because this criterion is quadratic. Additionally in practice the wavefront noise covariance matrix is taken as $C_{n'} = \sigma_{n'}^2 I$ (where I denotes the identity matrix) so that $J_s = \frac{1}{2\sigma_{n'}^2} \|\mathbf{s}_t - \mathcal{D}\boldsymbol{\phi}_t\|^2$ and its gradient reads:

$$\frac{dJ_s}{d\boldsymbol{\phi}_t} = \frac{1}{\sigma_{n'}^2} \mathcal{D}^T (\mathcal{D}\boldsymbol{\phi}_t - \mathbf{s}_t). \tag{A6}$$

Similarly, the gradient of $J_\phi = \frac{1}{2} \boldsymbol{\phi}_t^T C_\phi^{-1} \boldsymbol{\phi}_t$ reads:

$$\frac{dJ_\phi}{d\boldsymbol{\phi}_t} = C_\phi^{-1} \boldsymbol{\phi}_t. \tag{A7}$$

ACKNOWLEDGMENTS

This work was supported by contracts from SPOTI, Ministère de la Défense, France. The authors thank Thierry Fusco, Gérard Rousset, Jérôme Idier and Amandine Blanc for fruitful discussions. Many thanks also to Ruy Deron, Joseph Montri, Francis Mendez, Jean Lefèvre, Didier Rabaud, Christophe Coudrain, who made the experimental setup happen. Corresponding author Laurent Mugnier can be reached by e-mail at `Laurent.Mugnier@onera.fr`.

1. J.-C. Fontanella. Analyse de surface d'onde, déconvolution et optique active. *J. of Optics (Paris)*, 16(6):257–268, 1985.
2. J. Primot, G. Rousset, and J.-C. Fontanella. Image deconvolution from wavefront sensing: atmospheric turbulence simulation cell results. In M.-H. Ulrich, editor, *Very Large Telescopes and their Instrumentation, Volume II*, number 30 in ESO Conference and Workshop Proceedings, pages 683–692, Garching bei München, Germany, 1988. ESO.
3. J. Primot, G. Rousset, and J.-C. Fontanella. Deconvolution from wavefront sensing: a new technique for compensating turbulence-degraded images. *J. Opt. Soc. Am. A*, 7(9):1598–1608, 1990.
4. J. D. Gonglewski, D. G. Voelz, J. S. Fender, D. C. Dayton, B. K. Spielbusch, and R. E. Pierson. First astronomical application of postdetection turbulence compensation: images of α aurigae, ν ursae majoris, and α geminorum using self-referenced spechle holography. *Appl. Opt.*, 29(31):4527–4529, 1990.
5. T. Marais, V. Michau, G. Fertin, J. Primot, and J. C. Fo ntanella. Deconvolution from wavefront sensing on a 4 m telescope. In J. M. Beckers and F. Merkle, editors, *High-Resolution Imaging by Interferometry II, part I*, number 39 in ESO Conference and Workshop Proceedings, pages 589–597, Garching bei München, Germany, March 1992. ESO.
6. F. Roddier. Passive versus active methods in optical interferometry. In F. Merkle, editor, *High-resolution imaging by interferometry, part II*, number 29 in ESO Conference and Workshop Proceedings, pages 565–574, Garching bei München, Germany, July 1988. NOAO-ESO.
7. M. C. Roggemann, C. A. Hyde, and B. M. Welsh. Fourier phase spectrum estimation using deconvolution from wavefront sensing and bispectrum reconstruction. In *Adaptive optics*, volume 12 of *Technical Digest Series*, pages 133–135, Washington, 1996. OSA, OSA.

8. D. Dayton, J. Gonglewski, and S. Rogers. Experimental measurements of estimator bias and the signal-to-noise ratio for deconvolution from wave-front sensing. *Appl. Opt.*, 36(17):3895–3903, 1997.
9. M. C. Roggemann and B. M. Welsh. Signal to noise ratio for astronomical imaging by deconvolution from wave-front sensing. *Appl. Opt.*, 33(23):5400–5414, August 1994.
10. M. C. Roggemann, B. M. Welsh, and J. Devey. Biased estimators and object-spectrum estimation in the method of deconvolution from wave-front sensing. *J. Opt. Soc. Am. A*, 13(24):5754–5763, August 1994.
11. J.-M. Conan, V. Michau, and G. Rousset. Signal-to-noise ratio and bias of various deconvolution from wavefront sensing estimators. In J. C. Dainty and L. R. Bissonnette, editors, *Image Propagation through the Atmosphere*, volume 2828, pages 332–339, Bellingham, Washington, 1996. Proc. Soc. Photo-Opt. Instrum. Eng., SPIE.
12. T. J. Schulz. Estimation-theoretic approach to the deconvolution of atmospherically degraded images with wavefront sensor measurements. In P. S. Idell, editor, *Digital Image Recovery and Synthesis II*, volume 2029, pages 311–320. Proc. Soc. Photo-Opt. Instrum. Eng., 1993.
13. L. M. Mugnier, J.-M. Conan, V. Michau, and G. Rousset. Imagerie à travers la turbulence par déconvolution myope multi-trame. In J.-M. Chassery and C. Jutten, editors, *Seizième Colloque sur le Traitement du Signal et des Images*, pages 567–570. GRETSI, September 1997.
14. D. C. Dayton, S. C. Sandven, and J. D. Gonglewski. Expectation maximization approach to deconvolution from wavefront sensing. In T. J. Schulz, editor, *Image Reconstruction and Restoration II*, volume 3170, pages 16–24. Proc. Soc. Photo-Opt. Instrum. Eng., October 1997.
15. L. M. Mugnier, C. Robert, J.-M. Conan, V. Michau, and S. Salem. Regularized multiframe myopic deconvolution from wavefront sensing. In M. C. Roggemann and L. R. Bissonnette, editors, *Propagation through the Atmosphere III*, volume 3763, pages 134–144, Bellingham, Washington, 1999. Proc. Soc. Photo-Opt. Instrum. Eng., SPIE.
16. T. Fusco, J.-M. Conan, V. Michau, L. M. Mugnier, and G. Rousset. Phase estimation for large field of view: application to multiconjugate adaptive optics. In M. C. Roggemann and L. R. Bissonnette, editors, *Propagation through the Atmosphere III*, volume 3763, pages 125–133, Bellingham, Washington, 1999. Proc. Soc. Photo-Opt. Instrum. Eng., SPIE.
17. T. Fusco, J.-M. Conan, V. Michau, L. Mugnier, and G. Rousset. Efficient phase estimation for large field of view adaptive optics. *Opt. Lett.*, 24(21), November 1999.
18. R. J. Noll. Zernike polynomials and atmospheric turbulence. *J. Opt. Soc. Am.*, 66(3):207–211, 1976.
19. D. M. Titterington. General structure of regularization procedures in image reconstruction. *Astron. Astrophys.*, 144:381–387, 1985.
20. G. Demoment. Image reconstruction and restoration: Overview of common estimation structures and problems. *IEEE Trans. Acoust. Speech Signal Process.*, 37(12):2024–2036, December 1989.
21. E. P. Wallner. Optimal wave-front correction using slope measurements. *J. Opt. Soc. Am. A*, 73(12):pp 1771–1776, December 1983.
22. B. M. Welsh and R. N. VonNiederhausern. Performance analysis of the self-referenced speckle-holography image-reconstruction technique. *Appl. Opt.*, 32(26):5071–5078, September 1993.
23. Harry L. Van Trees. *Detection, Estimation, and Modulation Theory. Part I: Detection, Estimation, and Linear Modulation Theory*. John Wiley & Sons, New York, 1968.
24. P. A. Bakut, V. E. Kirakosyants, V. A. Loginov, C. J. Solomon, and J. C. Dainty. Optimal wavefront reconstruction from a Shack-Hartmann sensor by use of a Bayesian algorithm. *Opt. Commun.*, 109:10–15, June 1994.
25. S. D. Ford, B. M. Welsh, and M. C. Roggemann. Constrained least-squares estimation in deconvolution from wave-front sensing. *Opt. Commun.*, 151:93–100, May 1998.
26. J.-M. Conan, L. M. Mugnier, T. Fusco, V. Michau, and G. Rousset. Myopic deconvolution of adaptive optics images using object and point spread function power spectra. *Appl. Opt.*, 37(21):4614–4622, July 1998.
27. L. P. Yaroslavsky and H. J. Caulfield. Deconvolution of multiple images of the same object. *Appl. Opt.*, 33(11):2157–2162, April 1994.
28. P. J. Green. Bayesian reconstructions from emission tomography data using a modified EM algorithm. *IEEE Trans. Med. Imag.*, 9:84–93, March 1990.
29. C. Bouman and K. Sauer. A generalized gaussian image model for edge-preserving map estimation. *IEEE Trans. Image Processing*, 2(3):296–310, July 1993.
30. W. J. J. Rey. *Introduction to robust and quasi-robust statistical methods*. Springer-Verlag, Berlin, 1983.
31. S. Brette and J. Idier. Optimized single site update algorithms for image deblurring. In *Proceedings of the International Conference on Image Processing*, pages 65–68, Los Alamitos, California, 1996. IEEE, IEEE Computer Society.
32. J.-M. Conan, T. Fusco, L. M. Mugnier, E. Kersalé, and V. Michau. Deconvolution of adaptive optics images with imprecise knowledge of the point spread function: results on astronomical objects. In D. Bonaccini, editor, *Astronomy with adaptive optics: present results and future programs*, number 56 in ESO Conference and Workshop Proceedings, pages 121–132, Garching bei München, Germany, February 1999. ESO/OSA.
33. T. Fusco, J.-P. Véran, J.-M. Conan, and L. Mugnier. Myopic deconvolution method for adaptive optics images of stellar fields. *Astron. Astrophys. Suppl. Ser.*, 134:1–10, January 1999.
34. T. J. Schulz. Multiframe blind deconvolution of astronomical images. *J. Opt. Soc. Am. A*, 10(5):1064–1073, 1993.
35. E. Thiébaut and J.-M. Conan. Strict *a priori* constraints for maximum-likelihood blind deconvolution. *J. Opt. Soc. Am. A*, 12(3):485–492, 1995.

36. Groupe Problèmes Inverses. Gpav : une grande œuvre collective. internal report, Laboratoire des Signaux et Systèmes, CNRS/Supélec/Université Paris-Sud, 1997.
37. D. P. Bertsekas. *Nonlinear programming*. Athena Scientific, Belmont, Massachussets, 1995.
38. D. G. Luenberger. *Introduction to linear and nonlinear programming*. Addison-Wesley, Reading, Massachussets, 1973.
39. Yu-Li You and M. Kaveh. A regularization approach to joint blur identification and image restoration. *IEEE Trans. Image Processing*, 5(3):416–428, March 1996.
40. N. Roddier. Atmospheric wavefront simulation using Zernike polynomials. *Opt. Eng.*, 29(10):1174–1180, 1990.
41. D. W. Tyler and C. L. Matson. Speckle imaging detector optimization and comparison. *Opt. Eng.*, 32(4):864–869, April 1993.
42. E. Thiébaut. Speckle imaging with the bispectrum and without reference star. In J. G. Robertson and W. J. Tango, editors, *International Astronomical Union Symposium on very high angular resolution imaging*, volume 158, page 209. Kluwer Academic Publishers, 1994.
43. R. G. Paxman, T. J. Schulz, and J. R. Fienup. Joint estimation of object and aberrations by using phase diversity. *J. Opt. Soc. Am. A*, 9(7):1072–1085, 1992.